Local epitaxial-like templating effects and grain size distribution in atomic layer deposited $Hf_{0.5}Zr_{0.5}O_2$ thin film ferroelectric capacitors

iD S. F. Lombardo, M. Tian, iD K. Chae, et al.

View Online   Export Citation   CrossMark

ARTICLES YOU MAY BE INTERESTED IN

Local epitaxial-like templating effects and grain size distribution in atomic layer deposited Hf$_{0.5}$Zr$_{0.5}$O$_2$ thin film ferroelectric capacitors

View Online   Export Citation   CrossMark

S. F. Lombardo,[1,a)] (iD) M. Tian,[2] K. Chae,[3,4] (iD) J. Hur,[5] N. Tasneem,[5] (iD) S. Yu,[5] K. Cho,[3] (iD) A. C. Kummel,[4]
J. Kacher,[1] (iD) and A. I. Khan[1,5] (iD)

AFFILIATIONS

[1] School of Materials Science and Engineering, Georgia Institute of Technology, 771 Ferst Dr. NW, Atlanta, Georgia 30332, USA
[2] Institute for Electronics and Nanotechnology, Georgia Institute of Technology, 345 Ferst Dr. NW, Atlanta, Georgia 30318, USA
[3] Department of Materials Science and Engineering, The University of Texas at Dallas, Richardson, Texas 75080, USA
[4] Department of Chemistry and Biochemistry, University of California, San Diego, La Jolla, California 92093, USA
[5] School of Electrical and Computer Engineering, Georgia Institute of Technology, 791 Atlantic Dr., Atlanta, Georgia 30332, USA

[a)] Author to whom correspondence should be addressed: slombardo6@getech.edu

ABSTRACT

The microstructure in fluorite-structure oxide-based ferroelectric thin films, especially when on standard semiconductor manufacturing platforms, is poly-/nano-crystalline, which controls the functionality, performance, and reliability of the device technologies based on them. Understanding the relationships between microstructure, process, and performance for this class of materials has remained challenging. Here, a systematic approach is presented for analyzing and visualizing grains, their size distributions, and interlayer templating effects in ferroelectric thin film systems by utilizing an advanced microscopy technique, namely nanobeam electron diffraction, coupled with dark-field transmission electron microscopy and atomic resolution scanning transmission electron microscopy. A 10 nm TiN/10 nm Hf$_{0.5}$Zr$_{0.5}$O$_2$ (HZO)/10 nm TiN ferroelectric heterostructure is probed. A geometric mean of the grain size in HZO of 26.8 nm ranging from 5 to 95 nm with top and bottom TiN layers having a much smaller grain size of approximately 6.8 nm ranging from 3 to 17 nm is observed. Furthermore, there is evidence of templating effects between HZO and TiN grain and domain boundaries showing [111] and [001] growth directions locally for HZO and TiN, respectively.

Published under an exclusive license by AIP Publishing. https://doi.org/10.1063/5.0057782

Ferroelectrics based on fluorite-structure oxides[1–3] have emerged as a highly attractive functional class of materials for next-generation device technologies, including ferroelectric random-access memories (FERAM),[4,5] nonvolatile ferroelectric field-effect transistors (FEFETs),[6] and negative capacitance field-effect transistors (NCFETs),[7,8] as a direct result of their exceptional scalability and compatibility with state-of-the-art complementary metal-oxide-semiconductor (CMOS) processes.[9,10] However, these ferroelectric materials are polycrystalline in a thin film form for which the microstructure can drastically vary, especially on high-volume semiconductor production platforms. Consequently, understanding the relationships between microstructure, process, and performance for this class of materials has particularly remained challenging. The polycrystalline microstructure plays an all-important role for the operation of ferroelectric memories, from multi-level cell capabilities and retention to reliability, endurance, and device-to-device

variation.[11–13] Microscopic features—interfacial dynamics, grain size, and orientation, etc.—play major roles in the thermodynamic phase stability leading to the characteristic ferroic responses observed in HfO$_2$-/ZrO$_2$-based capacitors.[14–19] Additionally, the microstructural properties of the capping layers and substrates used can impact the electrical and structural properties of hafnia-/zirconia-based ferroelectric thin films as a result of residual stresses, which can lead to the presence or absence of potential templating effects during synthesis, influencing the growth and, therefore, phase and texture of the resulting ferroelectric (and antiferroelectric) thin film, which is crucial for nonvolatile memories.[20–24] Furthermore, grain and sub-grain domain sizes change with increased scaling, influencing phase stability and the depth of variability among devices.[25–27]

Due to the complexity of the microstructure associated with these thin film materials, a wide range of advanced microscopy techniques

have been utilized to gain insight into the correlation between the microstructure and ferroelectric behavior. *In situ* STEM and high resolution transmission electron microscopy (HR-TEM) have been utilized for electrical biasing of ferroelectric (and antiferroelectric) thin film heterostructures in real time at the atomic scale to investigate the microstructural evolution and domain dynamics of polarization switching.[28–31] High-angle annular dark-field (HAADF) STEM imaging has been utilized to study phase as a result of field cycling behavior and dopant for HfO₂-based ferroelectric thin films.[32–34] Similarly, HAADF-STEM coupled with position average convergent beam electron diffraction (PACBED) has been used to determine phase associated with ferroelectricity[35] as well as investigate the atomic structures of grains and sub-grain domain boundaries[36] in doped hafnium oxide-based devices. Recently, near-coincident site epitaxy was reported in detail by Estandía *et al.* in ferroelectric, epitaxial HZO/LSMO thin film stacks via HAADF-STEM characterization.[37]

While these techniques allow for detailed probing of the local structure, at larger scales, they do not provide statistically significant insights. An additional microscopy technique, namely, transmission Kikuchi diffraction (TKD)—also termed transmission electron back-scattering diffraction (EBSD)—has recently been utilized by Lederer *et al.* to study and visualize the plan-view grain size, phase fraction, and orientation spanning several hundred nm² areas in ferroelectric HfO₂ thin films for grains as small as 10 nm.[38] Furthermore, Lederer *et al.* also probed the microstructure resulting from the interfacial layer of Si-doped HfO₂-based FEFETs over 1–2 μm² areas via TKD analysis as a function of annealing temperature, providing insight into the crystallization process.[39] Although TKD is a powerful tool for studying the grain structure over large areas, it is not without limitations: Size resolution is limited for ultrasmall grains as well as the ability to image cross sections of the entire thin film heterostructures (i.e., top and bottom metal electrodes). Conversely, NBED may be employed over large cross-sectional areas for statistical grain size analysis and visualization. Nano-beam electron diffraction is a state-of-the-art TEM technique used to acquire local diffraction information of a material with nanoscale resolution over length scales as large as 1–2 μm as well as high spatial resolution with an electron beam diameter reduced to as low as 1 nm, allowing for detailed analysis of grain size, phase, and orientation.[40–42]

Through systematic advanced microscopy characterization, the fundamental microstructural properties responsible for the FE electrical behavior observed in HZO thin films can be identified, bridging the gap in our understanding between structure–process–performance relationships. Here, a rigorous materials characterization approach is employed to understand grain size distribution and orientation resulting from the substrate microstructure in a TiN/HZO/TiN thin film stack, including detailed mapping of the grain structure via NBED analysis, a critical step in grain size engineering of future devices. NBED grain mapping and DF-TEM imaging are utilized to visualize and determine the grain size and distribution among TiN and HZO layers over several micrometers, along with HAADF-STEM to study local orientation and epitaxy at the HZO/TiN interface.

For the top and bottom electrodes, 12 nm-thick TiN layers were deposited at 250 °C by ALD (TiCl₄ + NH₃ plasma), with the starting wafer being heavily doped p-type Si. A 10 nm HZO layer was deposited in between TiN electrodes, without breaking vacuum. The oxygen source used for the HZO layer was O₂ plasma with background Ar

atmosphere at 80 ssc and 1.035 Å/cycle in a Cambridge NanoTech Fiji G2 Plasma Enhanced ALD (PEALD) system. For the HZO deposition, Tetrakis(dimethylamido)hafnium (TDMA-Hf) and tetrakis(dimethylamido)zirconium (TDMA-Zr) precursors were used, and the O₂ plasma power and dose were set to 5 s and 300 W, respectively. A post-deposition rapid thermal anneal in N₂ atmosphere was performed at 350 °C for 30 s to stabilize the ferroelectric properties of the HZO. Aluminum metal layers were e-beam evaporated to define the capacitor areas, which also served as a hard mask during subsequent wet etch (1:1 H₂O₂:H₂O at 55 °C) of the top TiN electrode. Electrical measurements were performed using a Keithley 4200-SCS. Electrical characteristics of these films were reported in Ref. 43.

Cross-sectional samples for (S)TEM imaging were prepared using an FEI Nova Nanolab 200 FIB/SEM equipped with a high-energy Focused Ion Beam (FIB) using Gallium-69 and operated at an accelerating voltage between 5 and 30 kV. The resulting FIB lamellas were approximately 20 μm in length with 5 μm windows thinned to approximately 50 nm in thickness. A Hitachi HD-2700 aberration-corrected STEM/SEM was used to capture atomic resolution STEM images, having a HAADF-STEM image resolution of 0.136 nm, operated at a 200 kV accelerating voltage, a 30 mrad convergence angle, and a beam current of 9 μA. NBED scans and dark-field TEM images were collected using a FEI Tecnai G2 F30 TEM/STEM operated at an accelerating voltage of 300 kV and a beam current of about 80–100 pA. A total of 140 DF-TEM images were collected over a length of approximately 5 μm along the cross section, each one requiring manual alignment of the objective aperture. In comparison, five NBED scans were collected over 400 × 40 nm cross section areas (2 μm total length) with a pixel size of 2 × 2 nm.

The HR-TEM image of the cross section of the Al/TiN/HZO/TiN/SiO₂ capacitor shows clear, uniform interfaces [Fig. 1(a)]. The polarization–voltage characteristics are shown for up to 10⁵ cycles in Fig. 1(b) in which steep, ferroelectric hysteresis loops are observed with ± 3.0 MV/cm. Atomic resolution STEM images indicate templating effects between the bottom TiN electrode and HZO thin film [Fig. 2(a)] in which the grain boundaries of the TiN grains align with domain boundaries of HZO grains. A schematic of this effect is shown
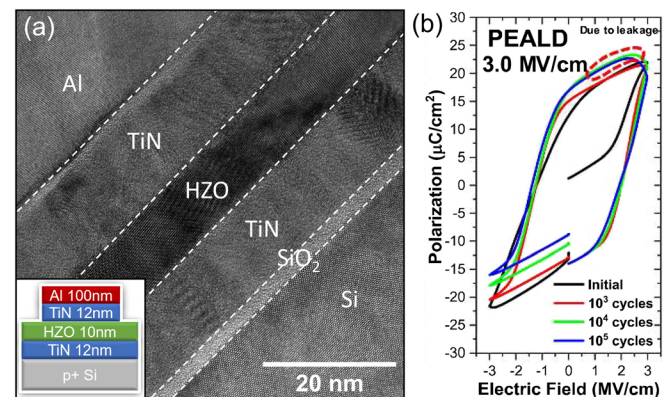

FIG. 1. (a) HR-TEM image of a 100 nm Al/12 nm TiN/10 nm HZO/12 nm TiN ferroelectric thin film stack over the 2 nm SiO₂/Si substrate and (b) corresponding polarization–electric field (P–E) switching characteristics for up to 10⁵ cycles for ± 3 MV/cm.
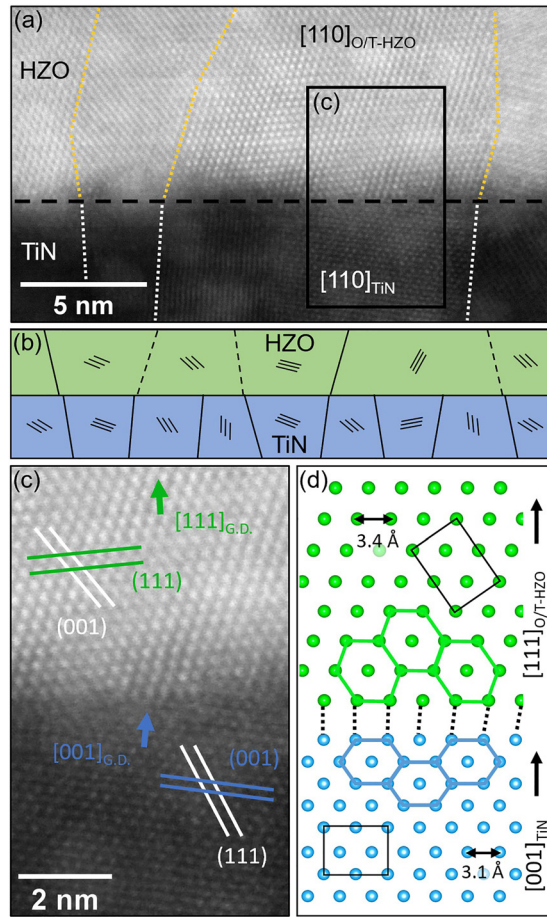
FIG. 2. (a) High-resolution STEM image of HZO over bottom TiN oriented along the [110] direction with HZO domain boundaries and TiN grain boundaries highlighted by gold and white dotted lines, respectively. (b) Domain and grain boundary schematic of templating effect for HZO and bottom TiN grains with domain and grain boundaries indicated by dotted and solid lines, respectively. (c) Expanded view of the HZO/TiN bottom interface with (111) and (001) planar symmetries indicated for each layer, and [111] and [001] growth directions indicated for HZO and TiN, respectively. (d) Atomic model of the projected (110) plane at the HZO/TiN interface, with lattice parameters being 3.4 and 3.1 Å for HZO (green atoms) and TiN (blue atoms), respectively, and black rectangles indicating unit cells.

in Fig. 2(b) in which the solid and dotted lines represent grain and domain boundaries, respectively. In ferroelectric, polycrystalline thin films, a grain—also termed crystallite—may be composed of multiple crystalline domains with slightly distorted unit cells and orientations, which typically form to relieve stress that arises due to the film being tethered to the substrate during the crystallization process and may have correlated alignment with ferroelectric switching domains.[44] The grain boundaries are formed by dislocations that separate regions of distinguishable crystallinity—phase, orientation, etc.—whereas domain boundaries separate regions of slightly distorted unit cells within a grain. There are, on average, approximately four TiN grains spanning the interface of a single HZO grain (consistent with the following DF-TEM and NBED grain size results), indicating a

relationship between the substrate grain structure and the presence of multiple crystalline domains within HZO grains as a result of potential templating effects. Both HZO and TiN atomic structures are oriented along the [110] direction with respect to the electron beam, with HZO being of either tetragonal or orthorhombic phase, which are solely indistinguishable from their respective fast Fourier transforms (FFTs) with respect to this orientation. An expanded view of the experimental and atomic model of the HZO/TiN interface projected along the [110] direction is shown in Figs. 2(c) and 2(d), respectively. The unit cells of each layer are indicted by the black rectangles. Hexagons are used to better visualize the relationship between the unit cells and growth directions. Here, the [111] growth direction of HZO and the [001] growth direction of TiN are aligned since the short edges of the hexagon of HZO atoms align with the long edges of the hexagon of TiN atoms. It is this configuration that generates the least lattice mismatch. The growth directions of the TiN and HZO indicate a local epitaxial relationship since the [001] direction provides a large degree of freedom with respect to epitaxial growth, as there are many similar crystallographic directions—one being the [111] direction—associated with the cubic family of directions. The [111] growth of HZO also coincides with the GI-XRD results in Fig. S1 for HZO, showing a characteristic o-111 peak near 30.5° 2θ (see the supplementary section for details). How prevalent such near-coincident site epitaxy is in heterostructures of fluorite structure oxides and what role such epitaxy play in determining their functional responses is an important question. NBED can be a powerful approach to understand such orientational relationships.

Dark-field TEM is utilized to capture individual crystallites along the HZO cross section. Here, a parallel, incident electron beam is transmitted through the films and a diffraction pattern is generated [Fig. 3(a)]. Specific reflection points within the pattern are then selected, using selected area diffraction (SAD) and objective apertures, to generate a dark-field image in which all crystallites associated with that reflection point appear bright, thus allowing us to discern individual grains from grain–grain overlap through the thickness of the sample. A DF-TEM image containing a variety of grains highlighted along each thin film is shown in Fig. 3(b) with examples of adjacent grains from the HZO and bottom TiN films with 12 and 7 nm grain sizes, respectively. A total of 65 grains from each film—top TiN, HZO, and bottom TiN—were analyzed to determine grain size distributions. Here, the grain size is measured as the longest width of the grain along the x-axis of the film. The distributions of each film are shown in Fig. 3(c). The geometric means of the top TiN, HZO, and bottom TiN were calculated to be 6.8, 26.8, and 6.8 nm, respectively (Table I). A wide range of grain sizes were measured for HZO, with the smallest and largest grains being approximately 5 and 95 nm, respectively, with the 90th percentile of grains being 58 nm. This is consistent with the ferroic response observed, as the ferroelectric phase is stabilized for larger grain sizes.[45] The top and bottom TiN electrode layers have similar size distributions, with sizes ranging between approximately 3–17 nm, with the 90th percentile of grains being roughly 10 nm. Although DF-TEM allows for local grain size analysis of each film for grains as small as 3 nm, NBED is more suitable for investigating larger length scales of the film.

To generate NBED grain maps for the purpose of grain size analysis, diffraction patterns are collected over a defined grid for off-line analysis. Here, virtual apertures are applied to diffraction patterns
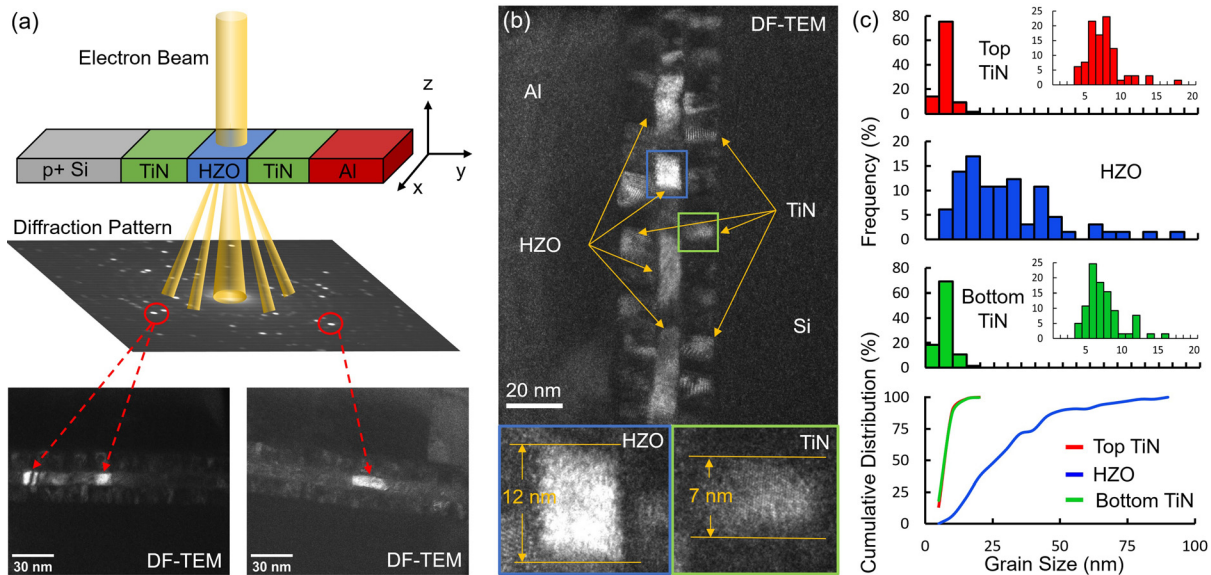
FIG. 3. (a) Dark-field TEM imaging schematic with dark-field images obtained from reflection points selected from diffraction patterns of the ferroelectric film. (b) Dark-field TEM image of the 12 nm TiN/10 nm HZO/12 nm TiN thin film stack showing highlighted grains from each film, with a single grain from HZO and TiN expanded having an approximate 12 and 7 nm grain size, respectively. (c) Grain size histograms calculated for top TiN, HZO, and bottom TiN (65 grains each) from the DF-TEM images, and the corresponding cumulative distribution functions for each layer.

collected from the HZO layer to form a series of virtual dark-field images, with the virtual aperture size being about 1–2 mrad. This analysis was performed using Gatan DigitalMicrograph software. Artificial color was randomly assigned to each virtual dark field image based on the maximum intensity of the selected reflection points using ImageJ software to distinguish between HZO grains and the NBED scan. The virtual dark field images were then overlayed after background subtraction to create a montage of grains. It is important to note that the reflection points from the HZO film may overlap with those from the TiN, so the color distributions are not exactly localized in HZO. Additionally, NBED maps were not generated with TiN grains included due to TiN having a much smaller grain size, which results in weaker reflection points from the diffraction pattern. These weak reflections could result in increased background noise when generating virtual dark-field images as opposed to measuring TiN grains from the real DF-TEM images directly. A STEM image with NBED scan area highlighted is displayed in Fig. 4(a) from which a grain map is

generated by selecting reflection points from various diffraction patterns associated with each grain along the scanned area. A total of 60 grains were measured from 5 NBED grain maps of 5 separate regions along the length of the HZO film. The grain size distribution obtained from these maps is shown in Fig. 4(b), with the geometric mean being approximately 28.1 nm and the 90th percentile of grains being approximately 67.6 nm. The other four grain maps [Fig. 4(c)] depict the variety of grain sizes among the HZO film, and grain sizes measured from all grains range between 7 and 96 nm. These values are consistent with those calculated from the DF-TEM analysis. These results are summarized in Table I. It is important to note here that grain size analysis from cross sections could result in underestimation of the grain size due to the random nature of cross sections. Larger sample sizes may improve the statistical significance of grain size obtained by this type of analysis. Conversely, adjacent grains of similar orientations could be interpreted as one, shifting the distribution to larger grain sizes. Nonetheless, NBED grain mapping can provide new insights into the grain size over several micrometers per sample, allowing for statistical analysis of grain sizes among ferroelectric and antiferroelectric thin film cross sections.

In conclusion, STEM images reveal local orientation and templating effects between the substrate and FE film in an ALD 10 nm TiN/10 nm HZO/10 nm TiN ferroelectric thin film heterostructure. A systematic approach was used to analyze and visualize grain sizes and distributions in ferroelectric thin film systems via nanobeam electron diffraction (NBED) coupled with dark-field transmission electron microscopy (DF-TEM). While the NBED and DF-TEM results statistically coincide, NBED can provide additional information, including statistically meaningful epitaxial relationships. At this point, it is important to note that this analysis relies on two-dimensional through-thickness projections of the cross section. Combining NBED

TABLE I. Grain size geometric means ($\prod$) with standard deviations and cumulative distributions of 10% (d10), 50% (d50), and 90% (d90) for top TiN, HZO, and bottom TiN layers from DF-TEM images (65 grains each) and NBED grain maps (60 grains).

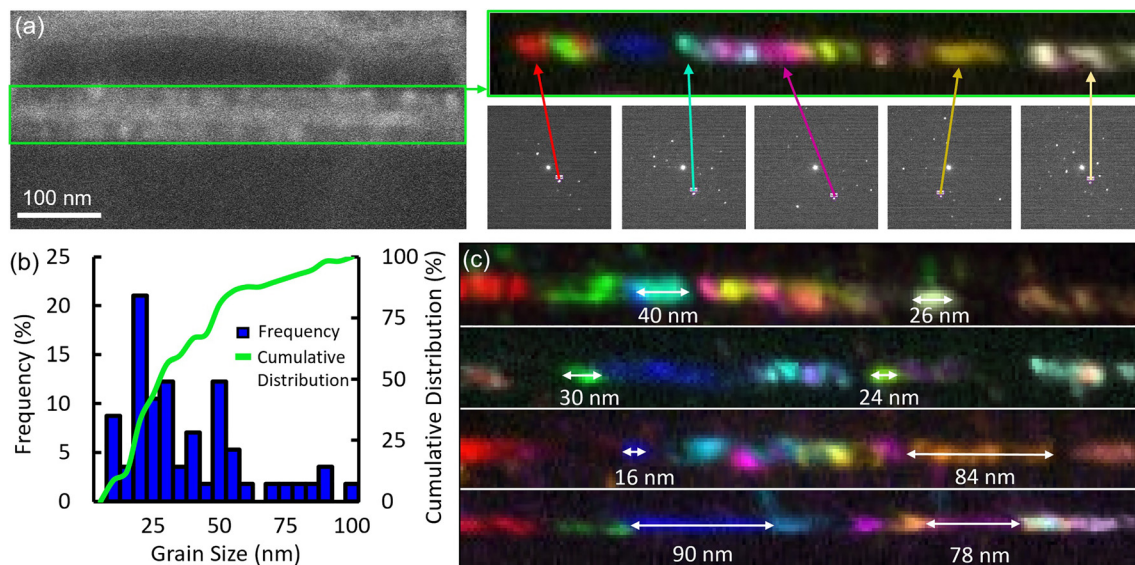| Grain size	DF-TEM			NBED
	Top TiN	$Hf_{0.5}Zr_{.05}O_2$	Bottom TiN	$Hf_{0.5}Zr_{.05}O_2$
$\prod$	6.8 ± 1.3 nm	26.8 ± 1.7 nm	6.8 ± 1.3 nm	28.1 ± 1.9 nm
d10	4.8 nm	12.8 nm	4.7 nm	11.1 nm
d50	6.7 nm	26.1 nm	6.5 nm	28.7 nm
d90	9.8 nm	57.7 nm	10.8 nm	67.6 nm

FIG. 4. (a) STEM image with the NBED scan area outlined in green and the corresponding grain map obtained where each grain is identified using reflection points selected from diffraction patterns associated with various positions along the length of the scan area. (b) Grain size histogram and cumulative distribution function obtained from 60 grains measured from the NBED grain maps. (c) NBED grain maps generated from different regions along the TEM cross section sample with a wide range of grain sizes measured.

with other advanced microscopy techniques, such as TKD, *in situ* TEM, and atomic scale tomography, may allow for three-dimensional analysis, providing further details of the grain structure and interfacial properties within these thin film material systems. Such studies enable engineering of electrode/substrate microstructure, leading to precise control of the resulting grain size, texture, and phase in nanoscale ferroelectric and antiferroelectric thin films for use in innovative memory device technologies in the coming years.

See the supplementary material for GI-XRD results of the studied HZO ferroelectric thin film.

DATA AVAILABILITY

The data that support the findings of this study are available from the corresponding author upon reasonable request.

REFERENCES

[1]T. S. Böscke, J. Müller, D. Bräuhaus, U. Schröder, and U. Böttger, "Ferroelectricity in hafnium oxide thin films," Appl. Phys. Lett. **99**, 102903 (2011).

[2]D. Bräuhaus, S. Mueller, U. Schröder, U. Böttger, L. Frey, T. S. Böscke, T. Mikolajick, and J. Müller, "Ferroelectricity in simple binary ZrO_2 and HfO_2," Nano Lett. **12**, 4318–4323 (2012).

[3]J. Müller, T. S. Böscke, D. Bräuhaus, U. Schröder, U. Böttger, J. Sundqvist, P. Kcher, T. Mikolajick, and L. Frey, "Ferroelectric $Zr_{0.5}Hf_{0.5}O_2$ thin films for nonvolatile memory applications," Appl. Phys. Lett. **99**, 112901 (2011).

[4]H. Ishiwara, "Ferroelectric random-access memories," J. Nanosci. Nanotechnol. **12**, 7619–7627 (2012).

[5]M. H. Park, Y. H. Lee, T. Mikolajick, U. Schroeder, and C. S. Hwang, "Review and perspective on ferroelectric HfO_2-based thin films for memory applications," MRS Commun. **8**, 795–808 (2018).

[6]A. I. Khan, A. Keshavarzi, and S. Datta, "The future of ferroelectric field-effect transistor technology," Nat. Electron. **3**, 588–597 (2020).

[7]X. Li, J. Sampson, A. Khan, K. Ma, S. George, A. Aziz, S. K. Gupta, S. Salahuddin, M. F. Chang, S. Datta, and V. Narayanan, "Enabling energy-efficient nonvolatile computing with negative capacitance FET," IEEE Trans. Electron Devices **64**, 3452–3458 (2017).

[8]H. Agarwal, P. Kushwaha, Y. K. Lin, M. Y. Kao, Y. H. Liao, A. Dasgupta, S. Salahuddin, and C. Hu, "Proposal for capacitance matching in negative capacitance field-effect transistors," IEEE Electron Device Lett. **40**, 463–466 (2019).

[9]M. Hoffmann, M. Pešić, K. Chatterjee, A. I. Khan, S. Salahuddin, S. Slesazeck, U. Schroeder, and T. Mikolajick, "Direct observation of negative capacitance in polycrystalline ferroelectric HfO_2," Adv. Funct. Mater. **26**, 8643–8649 (2016).

[10]T. S. Böscke, J. Müller, D. Bräuhaus, U. Schröder, and U. Böttger, "Ferroelectricity in hafnium oxide: CMOS compatible ferroelectric field effect transistors," in *International Electron Device Meeting-Technical Digest* (IEEE, 2011), pp. 547–550.

[11]S. J. Kim, J. Mohan, H. S. Kim, J. Lee, C. D. Young, L. Colombo, S. R. Summerfelt, T. San, and J. Kim, "Low-voltage operation and high endurance of 5-nm ferroelectric $Hf_{0.5}Zr_{0.5}O_2$ capacitors," Appl. Phys. Lett. **113**, 182903–182904 (2018).

[12]S. Mueller, S. Slesazeck, T. Mikolajick, J. Müller, P. Polakowski, and S. Flachowsky, "Next-generation ferroelectric memories based on FE-HfO_2," in ISAF, ISIF, and Piezoelectric Force Microscopy Workshop (PFM) (2015).

[13]S. Dünkel, M. Trentzsch, R. Richter, P. Moll, C. Fuchs, O. Gehring, M. Majer, S. Wittek, B. Müller, T. Melde, H. Mulaosmanovic, S. Slesazeck, S. Müller, J. Ocker, M. Noack, D.-A. Löhr, P. Polakowski, J. Müller, T. Mikolajick, J. Höntschel, B. Rice, J. Pellerin, and S. Beyer, "A FeFET based super-low-power ultra-fast embedded NVM technology for 22 nm FDSOI and beyond," in *International Electron Device Meeting* (IEEE, 2017).

[14]S. Clima, D. J. Wouters, C. Adelmann, T. Schenk, U. Schroeder, M. Jurczak, and G. Pourtois, "Identification of the ferroelectric switching process and dopant-dependent switching properties in orthorhombic HfO_2: A first principles insight," Appl. Phys. Lett. **104**, 092906 (2014).

[15]T. D. Huan, V. Sharma, G. A. Rossetti, and R. Ramprasad, "Pathways towards ferroelectricity in hafnia," Phys. Rev, B **90**, 064111 (2014).

[16]R. Materlik, C. Kunneth, and A. Kersch, "The origin of ferroelectricity in $Hf_{1-x}Zr_xO_2$: A computational investigation and a surface energy model," J. Appl. Phys. **117**, 134109 (2015).

[17]S. Choudhury, Y. L. Li, C. Krill, and L. Q. Chen, "Effect of grain orientation and grain size on ferroelectric domain switching and evolution: Phase field simulations," Acta Mater. **55**, 1415–1426 (2007).

[18]R. Batra, T. D. Huan, J. L. Jones, G. Rossetti, and R. Ramprasad, "Factors favoring ferroelectricity in hafnia: A first-principles computational study," J. Phys. Chem. C **121**, 4139–4145 (2017).

[19]M. H. Park, H. J. Kim, Y. J. Kim, T. Moon, and C. S. Hwang, "The effects of crystallographic orientation and strain of thin $Hf_{0.5}Zr_{0.5}O_2$ film on its ferroelectricity," Appl. Phys. Lett. **104**, 072901 (2014).

[20]S. J. Kim, D. Narayan, J. G. Lee, J. Mohan, J. S. Lee, J. Lee, H. S. Kim, Y. C. Byun, A. T. Lucero, C. D. Young, S. R. Summerfelt, T. San, L. Colombo, and J. Kim, "Large ferroelectric polarization of $TiN/Hf_{0.5}Zr_{0.5}O_2/TiN$ capacitors due to stress-induced crystallization at low thermal budget," Appl. Phys. Lett. **111**, 242901 (2017).

[21]Y. Goh, J. Hwang, Y. Lee, M. Kim, and S. Jeon, "Ultra-thin $Hf_{0.5}Zr_{0.5}O_2$ thin-film-based ferroelectric tunnel junction via stress induced crystallization," Appl. Phys. Lett. **117**, 242901 (2020).

[22]Z. Wang, A. A. Gaskell, M. Dopita, D. Kriegner, N. Tasneem, J. Mack, N. Mukherjee, Z. Karim, and A. I. Khan, "Antiferroelectricity in lanthanum doped zirconia without metallic capping layers and post-deposition/-metallization anneals," Appl. Phys. Lett. **112**, 222902 (2018).

[23]Y. Lee, Y. Goh, J. Hwang, D. Das, and S. Jeon, "The influence of top and bottom metal electrodes on ferroelectricity of hafnia," IEEE Trans. Electron Devices **68**, 523–528 (2021).

[24]C.-Y. Wang, C.-I. Wang, S.-H. Yi, T.-J. Chang, C.-Y. Chou, Y.-T. Yin, and H.-C.-J. C. Lin, "Impact of a TiN capping layer on phase transformation and capacitance enhancement in ZrO_2," ACS Appl. Electron. Mater. **3**, 1937–1946 (2021).

[25]H. J. Kim, M. H. Park, Y. J. Kim, Y. H. Lee, W. Jeon, T. Gwon, T. Moon, K. D. Kim, and C. S. Hwang, "Grain size engineering for ferroelectric $Hf_{0.5}Zr_{0.5}O_2$ films by an insertion of Al_2O_3 interlayer," Appl. Phys. Lett. **105**, 192903 (2014).

[26]M. H. Park, H. J. Kim, Y. J. Kim, Y. H. Lee, T. Moon, K. D. Kim, S. D. Hyun, and C. S. Hwang, "Study on the size effect in $Hf_{0.5}Zr_{0.5}O_2$ films thinner than 8 nm before and after wake-up field cycling," Appl. Phys. Lett. **107**, 192907 (2015).

[27]J. Liao, B. Zeng, Q. Sun, Q. Chen, M. Liao, C. Qiu, Z. Zhang, and Y. Zhou, "Grain size engineering of ferroelectric Zr-doped HfO_2 for the highly scaled devices applications," IEEE Electron Device Lett. **40**, 1868–1871 (2019).

[28]C. H. Chiu, C. W. Huang, Y. H. Hsieh, J. Y. Chen, C. F. Chang, Y. H. Chu, and W. W. Wu, "In-situ TEM observation of multilevel storage behavior in low power FeRAM device," Nano Energy **34**, 103–110 (2017).

[29]S. Lombardo, C. Nelson, K. Chae, S. Reyes-Lillo, M. Tian, N. Tasneem, Z. Wang, M. Hoffmann, D. Triyoso, S. Consiglio, K. Tapily, R. Clark, G. Leusink, K. Cho, A. Kummel, J. Kacher, and A. Khan, "Atomic-scale imaging of polarization switching in an (anti-)ferroelectric memory material: Zirconia (ZrO_2)," in Symposium on VLSI Technology (IEEE, 2020).

[30]T. Chakrabortty, S. Matzen, H. W. Zandbergen, A. Björling, and D. Mannix, "Reversible oxygen migration and phase transitions in hafnia-based ferroelectric devices," Science **372**, 630–635 (2021).

[31]Q. Huang, Z. Chen, M. J. Cabral, F. Wang, S. Zhang, F. Li, Y. Li, S. P. Ringer, H. Luo, Y.-W. Mai, and X. Liao, "Direct observation of nanoscale dynamics of ferroelectric degradation," Nat. Commun. **12**, 2095 (2021).

[32]M. Pešić, F. P. G. Fengler, L. Larcher, A. Padovani, T. Schenk, E. D. Grimley, X. Sang, J. M. LeBeau, S. Slesazeck, U. Schroeder, and T. Mikolajick, "Physical mechanisms behind the field-cycling behavior of HfO_2-based ferroelectric capacitors," Adv. Funct. Mater. **26**, 4601–4612 (2016).

[33]E. D. Grimley, T. Schenk, X. Sang, M. Pešić, U. Schroeder, T. Mikolajick, and J. M. LeBeau, "Structural changes underlying field-cycling phenomena in ferroelectric HfO_2 thin films," Adv. Electron. Mater. **2**, 1600173 (2016).

[34]M. H. Park, T. Schenk, C. M. Fancher, E. D. Grimley, C. Zhou, C. Richter, J. M. Lebeau, J. L. Jones, T. Mikolajick, and U. Schroeder, "A comprehensive study on the structural evolution of HfO_2 thin films doped with various dopants," J. Mater. Chem. C **5**, 4677–4690 (2017).

[35]X. Sang, E. D. Grimley, T. Schenk, U. Schroeder, and J. M. Lebeau, "On the structural origins of ferroelectricity in HfO_2 thin films," Appl. Phys. Lett. **106**, 162905 (2015).

[36]E. D. Grimley, T. Schenk, T. Mikolajick, U. Schroeder, and J. M. LeBeau, "Atomic structure of domain and interphase boundaries in ferroelectric HfO_2," Adv. Mater. Interfaces **5**, 1701258 (2018).

[37]S. Estandía, N. Dix, M. F. Chisholm, I. Fina, and F. Sánchez, "Domain-matching epitaxy of ferroelectric $Hf_{0.5}Zr_{0.5}O_2$(111) on $La_{2/3}Sr_{1/3}MnO_3$(001)," Cryst. Growth Des. **20**, 3801–3806 (2020).

[38]M. Lederer, T. Kämpfe, R. Olivo, D. Lehninger, C. Mart, S. Kirbach, T. Ali, P. Polakowski, L. Roy, and K. Seidel, "Local crystallographic phase detection and texture mapping in ferroelectric Zr doped HfO_2 films by transmission-EBSD," Appl. Phys. Lett. **115**, 222902 (2019).

[39]M. Lederer, A. Reck, K. Mertens, R. Olivo, P. Bagul, A. Kia, B. Volkmann, T. Kämpfe, K. Seidel, and L. M. Eng, "Impact of the SiO_2 interface layer on the crystallographic texture of ferroelectric hafnium oxide," Appl. Phys. Lett. **118**, 012901 (2021).

[40]C. Gammer, V. Burak Ozdol, C. H. Liebscher, and A. M. Minor, "Diffraction contrast imaging using virtual apertures," Ultramicroscopy **155**, 1–10 (2015).

[41]N. Sorida, M. Takahashi, K. Dairiki, S. Yamazaki, and N. Kimizuka, "Nanometer-scale crystallinity in In-Ga-Zn-oxide thin film deposited at room temperature observed by nanobeam electron diffraction," Jpn. J. Appl. Phys., Part 1 **53**, 115501 (2014).

[42]O. Panova, X. C. Chen, K. C. Bustillo, C. Ophus, M. P. Bhatt, N. Balsara, and A. M. Minor, "Orientation mapping of semicrystalline polymers using scanning electron nanobeam diffraction," Micron **88**, 30–36 (2016).

[43]J. Hur, N. Tasneem, G. Choe, P. Wang, Z. Wang, A. I. Khan, and S. Yu, "Direct comparison of ferroelectric properties in $Hf_{0.5}Zr_{0.5}O_2$ between thermal and plasma-enhanced atomic layer deposition," Nanotechnology **31**, 505707 (2020).

[44]Y. Ivry, D. Chu, J. F. Scott, and C. Durkan, "Domains beyond the grain boundary," Adv. Funct. Mater. **21**, 1827–1832 (2011).

[45]M. H. Park, Y. H. Lee, H. J. Kim, T. Moon, K. D. Kim, S. D. Hyun, T. Mikolajick, U. Schroeder, and C. S. Hwang, "Understanding the formation of the metastable ferroelectric phase in hafnia-zirconia solid solution thin films," Nanoscale **10**, 716–725 (2018).